Numerical modelling of a box-type bottom-detached oscillating water column wave energy conversion device: a comparison of experimental data with BEM and CFD numerical modelling

Vaibhav Raghavan, Irene Simonetti, George Lavidas, Andrei Metrikine, and Lorenzo Cappietti

Abstract—**Utilization of Boundary Element Method (BEM) based on linear potential flow for modelling Oscillating Water Column (OWC) devices has gained popularity in the last two decades. The commercial BEM solver WAMIT has been used widely for modelling OWCs and validated using experimental modelling. Literature has shown that when using the thin disk approach for modelling the imaginary piston in OWCs in BEM solver Nemoh, the results have been poor since the solver fails to provide good results when the source and field points are very close. In this research, the two-body interaction problem has been adopted in modelling a box-type and bottom-detached OWC device in Nemoh, where the first modelled body is the OWC hull (fixed) and the second body is an imaginary piston modelled to the same length as the internal water column. An average linear damping coefficient relating pressure and discharge is used within a frequency domain model and the obtained response is compared with experimental data. A direct comparison is also conducted with the numerical method of Computational Fluid Dynamics (CFD), which has shown to be accurate for modelling OWC devices, however it does require significantly higher computational resources. A two-dimensional CFD numerical wave tank which allows for wave generation and absorption has been implemented within the open-source package OpenFOAM® and is used for comparative purposes. Results show that while CFD matches well with the experimental results, the BEM model under-estimates the response. To further improve this, an instantaneous frequency dependent damping coefficient relating pressure and discharge is derived, which then provides very close results to both the experiments and CFD model.**

Keywords—**Oscillating Water Column, Boundary Element Method, Computational Fluid Dynamics, Nemoh**

I. Introduction

ENERGY conversion could potentially accelerate the process of energy transition towards zero-carbon, contributing to a climate-neutral energy supply. At present, the technological development of Wave Energy Conversion (WEC) is limited by several technical and non-technical issues, as, e.g., the need to reduce the Levelized Cost of Energy (LCOE) and to increase the expected survivability of the device under extreme wave conditions. Reliable and accurate numerical modelling tools are fundamental in order to provide estimations of the key performance indicators of a WEC, which are in turn essential to support investment in decision-making process to drive the sector development.

Among the different technologies for wave energy conversion, the Oscillating Water Column (OWC) has the strong advantage of structural simplicity and robustness, and it is generally considered as one of the most promising technologies [1]. In its basic not-floating version, the OWC comprises of a hydraulic structure, a hollow caisson made of concrete or steel, provided with an underwater opening for the interaction with the incident waves and an upstaging air chamber connected to a duct embedding an air turbine. The sea waves incident on the caisson cause an oscillating heave motion of the inner column of water, that alternatively compresses and expands the upstanding air, driving an airflow through the turbine.

Utilization of BEM methods for modelling OWC devices has gained popularity in the last two decades. Most literature indicates the use of BEM has been performed with the industrial standard solver WAMIT, particularly when doing experimental validations. To this extent, WAMIT is also the most developed BEM solver for OWCs as it offers the ability to model the OWC is two different ways – 1) The imaginary piston above the internal water column modelled as a thin massless disk in combination with generalized degrees of freedom that can use all 6 modes 2) The second method models the outer body (OWC hull) and the imaginary piston in place of the water column in a two-body system, where the length of the piston is varied. This is particularly useful when the water column moves only in heaving.

The first method (generalized degrees of freedom approach) was adapted in [2] where BEM was used for performing a 3D hydrodynamic analysis of an

The work has been a part of the EU-SCORES project that has received funding from the European Union's Horizon 2020 research and innovation programme under grant agreement No 101036457.

V. Raghavan (e-mail: v.raghavan@tudelft.nl), G. Lavidas (e-mail: g.lavidas@tudelft.nl) and A. Metrikine (A.Metrikine@tudelft.nl) are with the Marine Renewable Energies Lab (MREL) from the Offshore Engineering Group in the Delft University of Technology, Netherlands. I. Simonetti (irene.simonetti@unifi.it) and L. Cappietti (lorenzo.cappietti@unifi.it) are with the Laboratorio di Ingegneria Marittima (LABIMA) at the University of Florence, Italy.

Digital Object Identifier:
https://doi.org/10.36688/ewtec-2023-142

oscillating water column wave power plant. Experimental validation was performed with the BEM solver WAMIT for the diffraction amplitude as well as the power production from the power plant. Similarly, [3] adapted the same method for the hydrodynamic analysis utilizing WAMIT for a double OWC chamber. Experimental validations were performed with respect to the free surface oscillation in the chamber as well as the pressure drop across the orifice, which were well captured with the model.

Using the two-body approach, [4] performed a hydrodynamic analysis using WAMIT of a cylindrical oscillating water column focusing on the length of the imaginary piston in place of the water column. Although WAMIT is capable of performing calculations with a thin disk model, when using a piston type model, it was shown that accurate predictions for the internal water column surface oscillation comparing frequency, and time domain responses were obtained when utilizing the entire length of the water column as the length of the piston. The non-linearities due to the pressure above the water column could then be captured more effectively when solving the system in the time domain.

[5] modelled an OWC device with the massless disk method as well as a two-body method using Nemoh and compared it with WAMIT. Nemoh is incapable of utilizing the massless disk method as it fails to provide results for the hydrodynamic coefficients when modelling thin elements [5]. However, when the two-body system was used, Nemoh gave results close to that of WAMIT particularly when the length of the imaginary piston is equal to the length of the water column. This was also observed by [4], where the piston modelled to the full length of the water column gave close results both in time domain and frequency domain.

The use of high-fidelity modelling approaches based on Computational Fluid Dynamics (CFD) for simulating OWC devices has been gaining an increasing diffusion over the last decade [6]. Despite a considerable increase in the computational time compared to BEM-based approaches, CFD simulations of the OWC device allow for consideration of the hydrodynamic interaction between the device and the incident waves accounting for multiphase, real fluid and nonlinear effects (including viscous losses, turbulence, wave breaking phenomena, nonlinear effects due to the presence of the PTO system). The CFD approach has been mainly adopted to assess the effect of specific design parameters of the OWC on the hydrodynamic conversion potentiality of the device and for design optimization (e.g., [7] ; [8])

The vast majority of the CFD applications in the literature are based on solving Reynolds-averaged Navier–Stokes (RANS) equations, while the use of Large Eddy Simulations (LES) is more limited (e.g. [8]; [9]). Both two-dimensional ([10]; [11]; [12]) or three-dimensional ([13]; [14]; [15]) CFD-based Numerical Wave Tanks (NWT) have been applied and successfully validated by means of comparison with laboratory data, showing relative errors on the inner free surface oscillation and relative air pressure in the OWC camber generally within a range of 5-15% with experimental data. To the author's knowledge there is no experimental validation study performed with BEM solver Nemoh for OWC devices or a comparison of BEM with more advanced methods such as CFD for OWC devices. Hence the authors chose to utilize Nemoh and CFD for a numerical comparison. The model was created using Nemoh based on modelling the imaginary piston to the length of the water column. The detailed background theory and features of Nemoh are discussed in [16], [5] and [17].

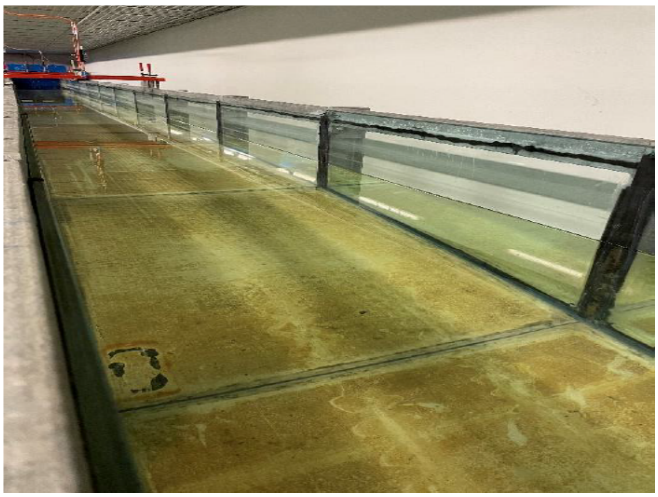

Fig. 1. LABIMA-WCF Wave tank

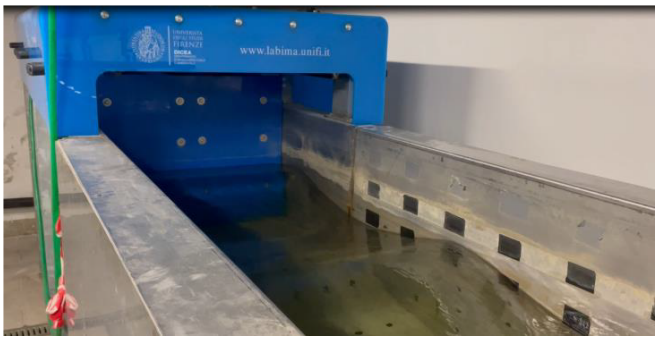

Fig. 2. LABIMA-WCF piston type wave generator

II. Experimental Setup

The BOX model was created based on designs from LABIMA and installed in the Wave-Current flume One (LABIMA-WCF1). The LABIMA-WCF1 is a structure built entirely from steel and glass side walls, with a total length of 37.0 m and width and height of 0.8 m. The piston type wave generator is installed at one end of the wave flume, and it has a stroke equal to 1.5 m, driven by an electromechanical system with an absolute encoder of 0.01 cm accuracy of piston [18]. Fig. 1 shows the LABIMA-WCF1 wave tank and Fig. 2 shows the piston type wave generator.

The BOX model has a height of 0.527 m, length (along the wave direction) of 0.795 m and width (orthogonal to the wave direction) of 0.256 m. The plan and elevation of the model are shown in Fig. 3 and the

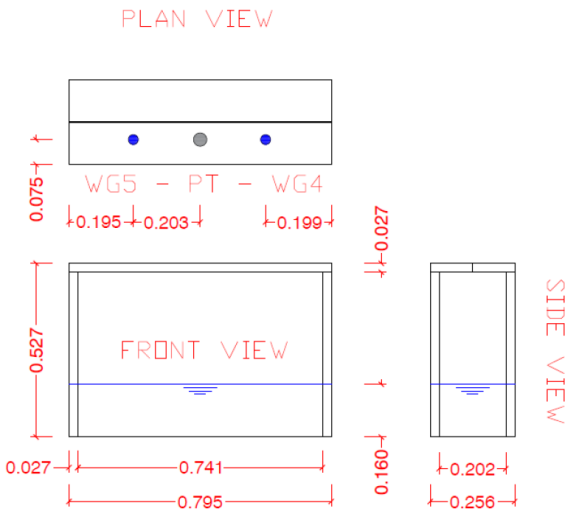

Fig. 3. BOX OWC device plan and elevation

Fig. 4. BOX OWC placed in tank - WG4 and WG5 are wave gauge designated by orange wires and PT is the pressure gauge depicted by the black wire

device as placed in the wave tank is shown in Fig. 4. The length was kept almost equal to the WCF1 width to set-up a fully 2D modelling thus avoiding the generation of transverse wave fields (e.g. wave reflection from the flume side walls). A slit of approximately 1.7 mm was created at the top of the BOX model to function as an orifice. The internal width of 0.2 m for the water column was so chosen to be within 30% of the maximum wavelength of the generated waves, thus allowing the internal free surface to oscillate almost completely in heave motion. This is motivated by the need to avoid sloshing phenomena in the OWC

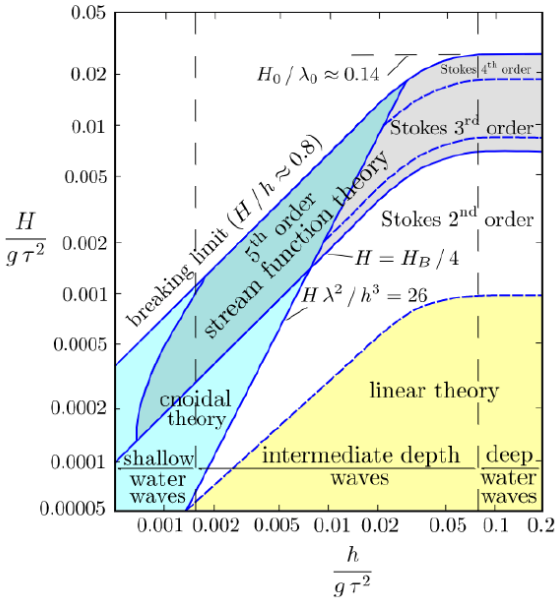

Fig. 5. Le Méhauté diagram [20]

chamber, which may be relevant when the ratio of the OWC internal width to the incident wavelength increases. Literature suggests that values of such a ratio exceeding approximately 1 to 4 should be avoided as discussed, e.g., in [19].

The BOX model was firmly fixed to the side walls such that the internal draft was 0.16 m. In Fig. 3, WG4 and WG5 refer to the wave gauges used to measure the displacement of the internal free surface with respect to the still water level inside, and PT is the pressure sensor used to measure the pressure fluctuations in the air pocket above the internal free surface.

Two test configurations were utilized. The first configuration was without the OWC model. This configuration was used to measure the testing wave conditions at the model location, in the absence of wave-structure interaction, which would later be used to test the OWC model. The second configuration was with the device installed.

III. Experimental Procedure

The test cases selected for the experiment were based on the Le Méhauté diagram (shown in Fig. 5), which shows the regions of applicability of the various wave conditions (i.e. linear and non-linear) for regular waves based on the water depth (h), wave height of the wave (H), wave length of the wave (λ) and time period (τ) of the wave.

10 regular wave cases were considered for this (see Table. I). The first four tests H01-H04 were performed to compare how BEM and CFD performed with various wave theories and cases H03, H05-10 were done keeping the wave height almost constant and varying the time period of the incident waves. This was to determine the Response amplitude operator (RAO) for the water column in the device under different wave steepness.

TABLE I
TEST MATRIX

Case name	Wave height, H (cm)	Wave period measured, τ (s)	Wave frequency, ω (rad/s)	Water depth, h (cm)	Wave theory
H01	1.10	1.43	4.39	50	Airy linear
H02	2.50	2.34	2.68	50	Airy linear
H03	6.60	1.43	4.39	50	Stokes 2^{nd} order
H04	9.30	1.43	4.39	50	Stokes 3^{rd} order
H05	6.30	1.00	6.28	50	Stokes 3^{rd} order
H06	6.40	1.20	5.23	50	Stokes 3^{rd} order
H07	6.50	1.60	3.93	50	Stokes 3^{rd} order
H08	6.00	1.80	3.49	50	Stokes 2^{nd} order
H09	6.10	2.00	3.14	50	Stokes 2^{nd} order
H10	6.10	2.20	2.85	50	Stokes 2^{nd} order

Fig. 6. Input for test case H01 to wavemaker

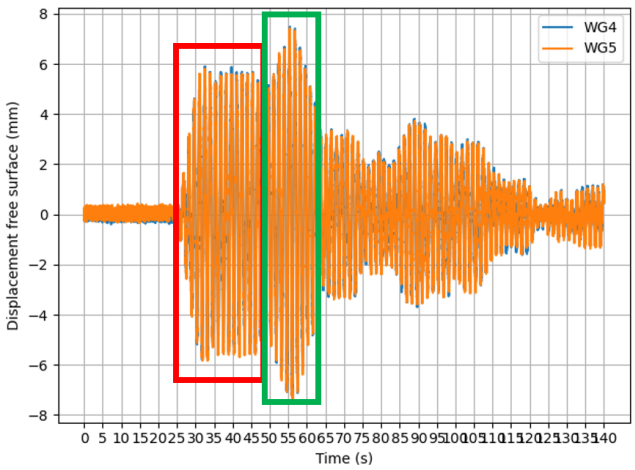

Fig. 7. Displacements measured by wave gauges WG4 and WG5 for the case H01. Within the red box, the incident waves are observed. Within the green box, a combination of incident and reflected waves can be seen.

The input for the wave maker was provided as an exponentially increasing sinusoidal curve starting from 0 to the desired wave height. As an example, the generated input conditions are shown in Fig. 6 for case H01. This was performed for all 10 cases.

The total period of input oscillations from the piston of the wave tank was chosen so as to capture the incident waves as well as the reflected waves at WG4 and WG5 (the right end of the tank has a reflecting wall). Fig. 7 shows the displacement as measured by the wave gauges WG4 and WG5 for the case H01.

The periods of oscillation within the red box indicate the time period when the generated waves from the piston pass WG4/WG5 in the absence of the reflected wave field coming from the end of the flume. Within the green box, the periods of oscillation of the incident waves together with the reflected waves can be observed, which are seen be interfere constructively with one another. The displacements of WG4 and WG5 within the red box (indicated in Fig. 7) are used to calculate the mean wave height and air discharge for each case.

A similar procedure as for WG4 and WG5 was used for PT to obtain the mean air pressure fluctuations. The pressure fluctuation for case H01 is shown in Fig. 8.

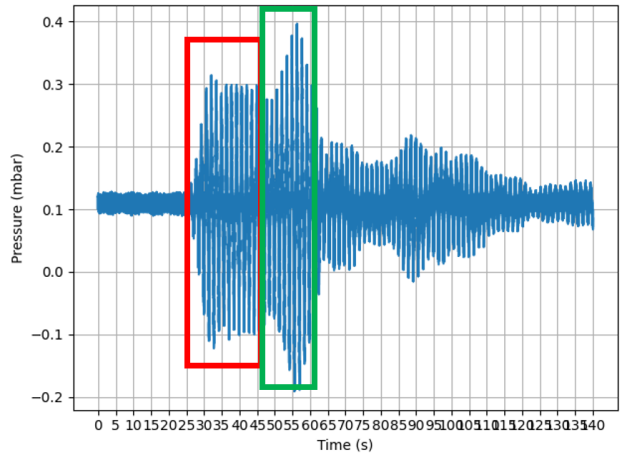

Fig. 8. Pressure measurement in pressure gauge PT for the case H01. Within the red box, the incident waves are observed. Within the green box, a combination of incident and reflected waves can be seen.

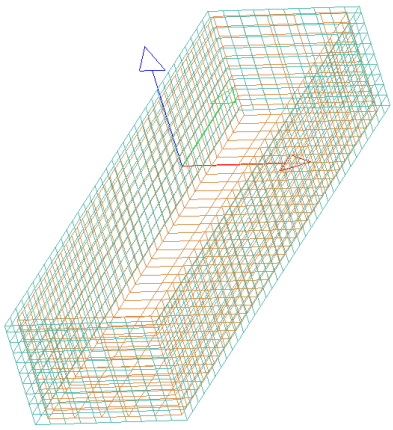

Fig. 9. Nemoh model BOX OWC device: BOX body (green) and imaginary piston (orange). The reference global axis is x(red) y(green) and z(blue)

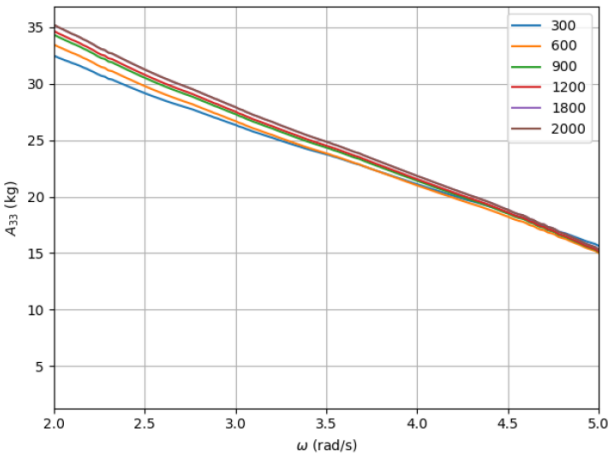

Fig. 10. Added mass with varying number of elements

IV. Numerical BEM Model Description

The numerical BEM model for the BOX OWC device was created based on the two-body system approach, where the submerged device hull was modelled as one fixed body and the imaginary piston in place of the water column was modelled as a second body. The imaginary piston is modelled to the length of the water column. The model is shown in Fig. 9. The dimensions are matched to those from the experimental model. The rectangular circumference of the body was modelled without a base, since the experimental model does not have a base as well. The piston was modelled with a base surface that is in contact with water.

The input wave frequencies were considered from 2 to 5 rad/s. This was done so to cover the frequencies in the experiments.

In order to decide on the number of elements required for discretizing the model, a convergence study was performed. The BEM solver provides the added mass, added damping (together known as the hydrodynamic coefficients) and excitation forces as the output. These parameters were utilized to perform the sensitivity analysis. The number of elements across the fixed body and piston were varied as 300, 600, 900, 1200, 1800 and 2000 elements. The results for the added mass, added damping and exciting forces are shown in Fig. 10, Fig. 11 and Fig. 12 respectively.

Based on these results, 2000 elements were selected since the difference with further increase in elements was negligible (convergence is reached) for all the parameters. After obtaining the hydrodynamic coefficients and exciting forces, the dynamic equation of motion for the model can be solved to obtain the displacement of the free surface. It should be noted that since the BEM model only considers the part of the body that is submerged in the water, the force due to the pressure above the internal free surface needs to be accounted for in another way. Therefore an additional pressure based forcing term is introduced into the final dynamic equation of motion for the device which results in (1).

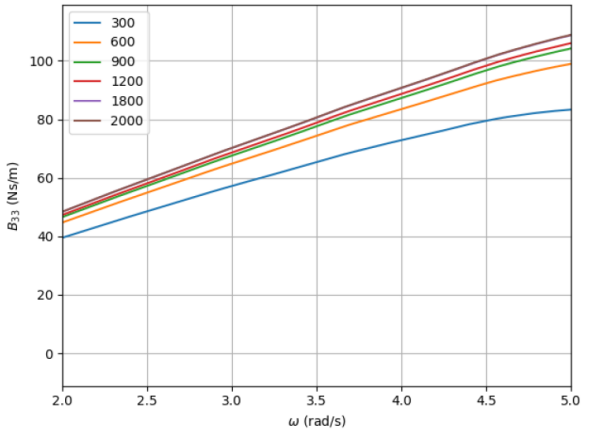

Fig. 11. Radiation damping with varying number of elements

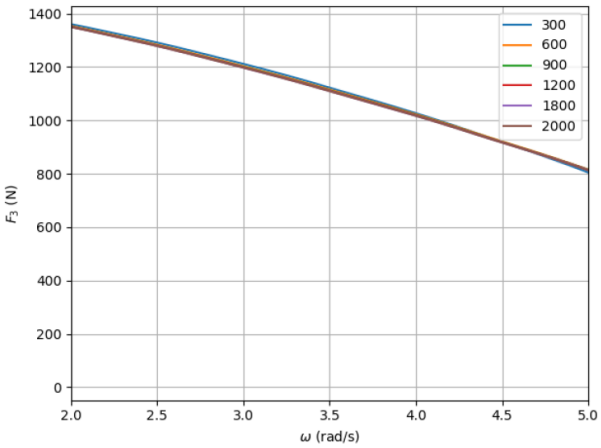

Fig. 12. Exciting force with varying number of elements

$$[i\omega(m_{33}+a_{33})+b_{33}+\frac{c_{33}}{i\omega}]v_3 = f_3 - A_0 p \quad (1)$$

where ω is the radial frequency (rad/s), m_{33} is the mass of the piston (kg) is the mass of the water column, a_{33} is the added mass of the piston (kg) obtained from Nemoh, b_{33} is the radiation damping (Ns/m) obtained from Nemoh, c_{33} is the hydrostatic restoring coefficient (N/m) (in this case for a box in heaving motion), v_3 is the complex amplitude of the velocity of the free surface (m/s), f_3 is the exciting force (N) obtained from Nemoh and $A_0 p$ is the force due to the pressure above the free surface where A_0 is the horizontal area of the free surface (m^2) and p is the complex amplitude of the pressure (N/m^2). The last term is the additional term due to the pressure.

The pressure can be computed from the discharge using a damping coefficient [4]. Since the considered methodology is in the frequency domain and fully linear, a linear relationship is assumed between the pressure and the discharge. Therefore, in the frequency domain, this can be written as follows:

$$p = kA_0 v_3 \quad (2)$$

Two approaches were considered for calculating the linear damping coefficient k for the pressure term. These are highlighted in the following section.

A. BEM model with averaged damping pressure coefficient

To calculate the damping coefficient k, the instantaneous velocity was used. In order to calculate the instantaneous velocity, first curve fitting was performed on the experimental displacement time series (see Fig. 7) using a sine curve.

The derivative of this curve provides the velocity of the free surface. This approach avoids the numerical errors in estimating the derivative by using the experimental time series of the free surface or pressure oscillations. A similar curve fitting was also performed for the experimental pressure time series, so that the instantaneous damping coefficient (absolute values) can be calculated for the considered time period by dividing the pressure by the discharge. The mean of the absolute values of the instantaneous damping coefficients in the considered time period was used to obtain as the estimate of the averaged damping coefficient k for each case. This is summarized in Table. II for the 10 cases.

In order to calculate the final average damping coefficient k, the mean of the average damping coefficients for the cases considered in creating the RAO (H3, H5-H9) was used.

B. BEM model with instantaneous frequency dependent damping pressure coefficient

The second approach for obtaining the damping coefficient k was to derive from the instantaneous damping coefficient (ratio of pressure and discharge) and do a curve fitting to obtain a relationship with the frequency of the incident wave. This was done in the following steps:

TABLE II
AVERAGED LINEAR DAMPING COEFFICIENT FOR PRESSURE

Case name	Averaged damping coefficient, k (kNs/m^5)
H01	1.045
H02	1.997
H03	28.140
H04	15.230
H05	7.440
H06	10.180
H07	7.600
H08	8.570
H09	8.360
H10	9.260

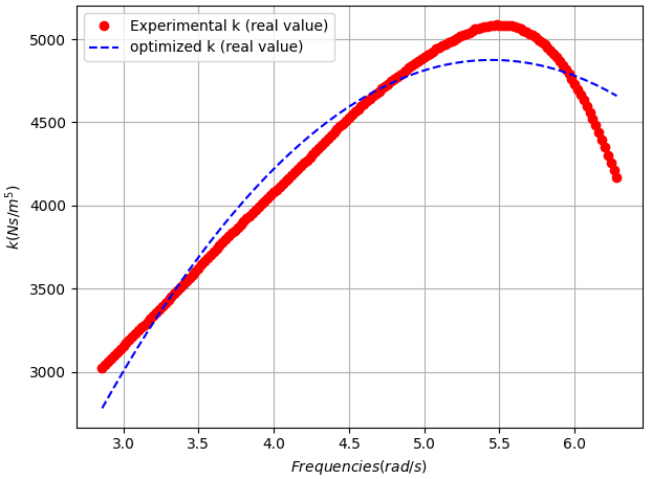

Fig. 13. Real part of the frequency dependent instantaneous damping coefficient

1) Based on the parameters of the numerical model i.e. the added mass, added damping, exciting forces, mass of the piston, restoring piston coefficient, and the experimental displacement of the piston, the complex value of the pressure damping coefficient was obtained in terms of these parameters. This is shown in (3).

$$k = [f_3 - [i\omega(m_{33}+a_{33})+b_{33}+\frac{c_{33}}{i\omega}]v_3]/A_0^2 v_3 \quad (3)$$

2) A complex frequency dependent damping coefficient is derived. The real and imaginary parts of the complex damping coefficient were fitted. A curve fitting is performed with a second order polynomial of the following form:

$$k(\omega) = (A_1+iA_2)\omega^2+(B_1+iB_2)\omega+(C_1+iC_2) \quad (4)$$

3) This result of the real and imaginary part of the instantaneous frequency dependent damping coefficient is shown in Fig. 13 and Fig. 14. The experimental k refers to the damping coefficient (real or imaginary) derived in step 1 using the experimental result, while the optimized k refers to the damping coefficient (real or imaginary) as obtained from the curve fitting performed in step 2.

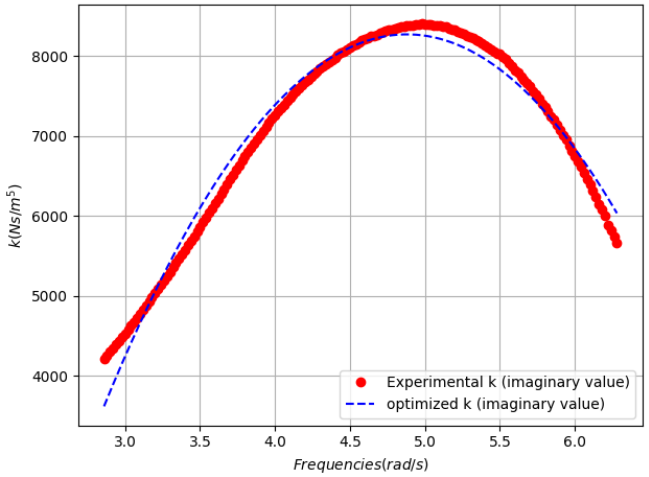

Fig. 14. Imaginary part of the frequency dependent instantaneous damping coefficient

V. Numerical CFD Model Description

The OWC was simulated in a two-dimensional CFD-based NWT implemented in the open-source environment OpenFOAM®. Mass conservation and RANS equations are solved for two, incompressible, phases (air and water) by using the Volume of Fluid (VOF) approach [21] with the interFoam solver. Stoke's second order wave theory has been used. In this approach, a transport equation is solved for the phase fraction γ. In the NWT, waves are generated and absorbed by prescribing boundary conditions for water levels and velocities according to the analytical expressions of a specified wave theory by using the IHFOAM [22]. In the present work, a stabilized version of the $k-\omega$ SST (Shear Stress Transport) turbulence model was used. Such a modified version of the standard $k-\omega$ SST model was developed to overcome the exponential growth of turbulent kinetic energy density and eddy viscosity under surface waves taking place in two equations turbulence models ensure, was adopted [23]. Such a turbulence model allows a stable long-term wave propagation over extended domains.

The PIMPLE algorithm is used for the coupling of the equations in the pressure-velocity system. The time step is dynamically adjusted to maintain a value of the Courant number Co<0.6 and a value of Co at the air-water interface αCo<0.6. The numerical schemes for the discretization of time derivatives are second-order accurate, blended with a first-order scheme to improve stability (the so-called CrankNicolson scheme in OpenFOAM®). The convection term in momentum equation is discretized with a central difference interpolation scheme, while the Monotone Upwind Scheme for Scalar Conservation Laws (MUSCL) interpolation scheme is used for the convection term in the transport equation of the phase fraction γ. The discretized system of equations is solved with a generalized Geometric-Algebraic Multi-Grid solver (GAMG).

The NWT has a length of 20 m (corresponding to 5-13·L, being L the incident wavelength), with the OWC located in the middle of it. The two-dimensional mesh is refined in the free surface zone (for an extension of

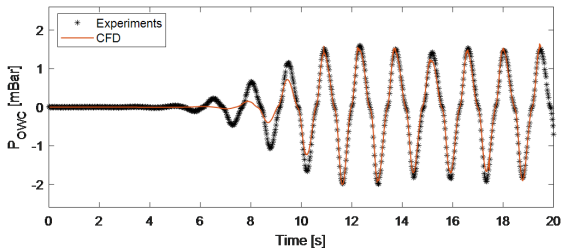

Fig. 15. Example of comparison of results from the CFD-NWT and experimental measurements of air pressure oscillation P_{OWC} for wave case H03

$\pm H$ around the still water level) with a resolution of around 12 cells per wave height H and a maximum cells aspect ratio equal to 2. The resulting mesh of the whole NWT has a size of approximately 450,000 cells. The mesh resolution in the free surface zone has been chosen based on sensitivity tests aimed at ensuring mesh independence for the wave propagation in the NWT (as discussed in [24] and [12]). In the near field of the OWC the mesh is farther refined. The length of the cells inside the OWC is ca. $W/120$, with W being the OWC chamber width). Around the slit on the top cover, the mesh has a resolution of about V/cells = 6, where V is the size of the slit (V=1.7 mm).

No-slip boundary conditions are used at the bottom of the NWT and on the OWC sidewalls. The water surface is set as an atmospheric pressure boundary. Velocity components and water surface elevations at the inlet/outlet are defined to introduce and absorb waves with IHFOAM.

VI. Results and Discussion

This section discusses the main results from the study in comparing the experiments, BEM and CFD.

A. Displacement of the free surface and Pressure variation

To compare the performance of the CFD-NWT and the BEM model in simulating the OWC, all wave cases were tested. For the CFD-NWT simulations, the equivalence of the incident wave conditions between laboratory experiments and numerical simulations was ensured by performing specific tests on wave propagation in the empty NWT, comparing the wave height in the OWC model position without any structure in the flume.

The comparisons were drawn through the relative differences in the peak of the OWC free surface oscillation and OWC chamber pressure oscillations with respect to the experiment for both BEM and CFD. For the BEM, the results based on the average linear damping coefficient k were used for the comparison here.

When considering the BEM model with the averaged damping coefficient, the relative error of the H_{OWC} of the free surface oscillation inside the OWC can go up to 0.16 (Table. III). The relative error on the height of the pressure oscillation inside the OWC chamber, ∇P_{OWC}, varies between 0.11 to 0.20 which is quite high. It is observed across all results that the BEM

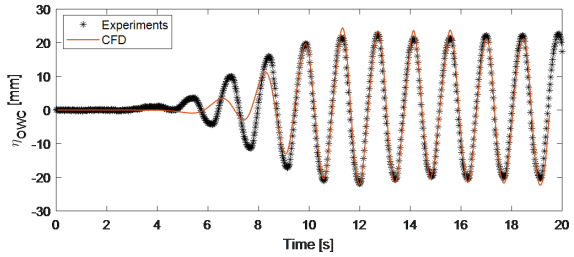

Fig. 16. Example of comparison of results from the CFD-NWT and experimental measurements of free surface oscillation η_{OWC} for wave case H03

TABLE III
RELATIVE ERROR BETWEEN EXPERIMENTAL TESTS AND BEM RESULTS (AVERAGED DAMPING COEFFICIENT) FOR THE HEIGHT OF FREE SURFACE OSCILLATION(H_{OWC}) AND HEIGHT OF THE PRESSURE OSCILLATION INSIDE THE OWC CHAMBER (∇P_{OWC})

Case name	Relative Error H_{OWC}[-]	Relative Error ∇P_{OWC}[-]
H01	0.12	0.15
H02	0.09	0.17
H03	0.15	0.15
H04	0.16	0.16
H05	0.09	0.20
H06	0.11	0.16
H07	0.11	0.16
H08	0.08	0.14
H09	0.08	0.11
H10	0.07	0.12

model considering the average damping coefficient always underestimates the results as compared to the experiments. Furthermore, since BEM here is a linear frequency domain model, the variation of the free surface oscillation and pressure oscillation is purely sinusoidal and is unable to capture some of the non-linear effects such as the second-order effects particularly observed in the pressure, the asymmetry in the crest and trough of the incident wave and the free surface response particularly seen in cases H04-H10 caused due to bottom friction effects at shallow depths, which are captured by the CFD simulation.

The agreement between experimental measurements and results of the simulations with the CFD-NWT is satisfactory for the wave cases considered (Fig. 15 and Fig. 16), with a relative error on the height H_{OWC} of the free surface oscillation inside the OWC up to -0.07, with negative values denoting a greater value in the experimental measurements (Table. IV). The relative error on the height of the pressure oscillation inside the OWC chamber, ∇P_{OWC}, varies between -0.03 and 0.14 (Table. IV). Even though the difference between laboratory tests and CFD results can be considered acceptable, it should be mentioned that a tendency towards an overestimation of the free surface oscillation and an underestimation of the pressure amplitude can be detected in most of the simulated wave conditions. Such systematic trend could be related to inaccuracy in manufacturing and/or measuring the exact value of the slit size in the laboratory model and to the subsequent difficulties in replicating such an exact value in the CFD-NWT. The response of the device, indeed, was found to be extremely sensitive to small variations in the size of the slit V, as highlighted in Fig. 17, where the RAO of the free surface oscillation inside the OWC obtained also with a slit size V=1.9 mm and 2.00 mm is comparatively depicted for the wave period τ =1.43 s.

TABLE IV
RELATIVE ERROR BETWEEN EXPERIMENTAL TESTS AND CFD-NWT FOR THE HEIGHT OF FREE SURFACE OSCILLATION(H_{OWC}) AND HEIGHT OF THE PRESSURE OSCILLATION INSIDE THE OWC CHAMBER (∇P_{OWC})

Case name	Relative Error H_{OWC}[-]	Relative Error ∇P_{OWC}[-]
H01	-0.06	0.13
H02	-0.07	0.04
H03	-0.07	0.04
H04	-0.05	0.03
H05	-0.02	0.02
H06	-0.05	-0.03
H07	-0.01	0.03
H08	0.03	0.08
H09	0.00	0.07
H10	-0.07	0.14

B. RAOs

The RAOs were computed for both BEM cases (with averaged damping coefficient and instantaneous frequency dependent damping coefficient) and compared with CFD-NWT and experimental results. These are shown in Fig. 17. When considering the BEM model with the averaged damping coefficient, the behaviour is similar to that of the experiments, however there is a consistent underestimation of the response in BEM as compared to the experiments. With regard to the other models, the CFD-NWT simulation considering the slit to be 1.7 mm thick and the BEM with the instantaneous frequency dependent damping coefficient give the closest results to the experiments.

Considering the instantaneous frequency dependent damping coefficient, it is interesting to see similarities with modelling of a linear turbine within the BEM formulation. [25], [26] and [27] modelled the linear turbine based on the mass transport equation considering air compressibility which results in a coefficient relating the pressure to the discharge(also referred to as the flow rate). This coefficient is complex in nature with the real part referring to the damping and the imaginary part with ω^2 that is regarded as the spring component. Since the imaginary part essentially has a restoring effect resulting from air compressibility [28], it is regarded as a spring in the system. The combination of stiffness and damping within the pressure term is partly reflected in the BEM formulation here with the instantaneous damping coefficient where the real and imaginary components (coefficients B_1, B_2, C_1 and C_2) contribute to stiffness and damping within the pressure term.

C. Computational resources

The computational time needed for the BEM simulations with Nemoh considering 2000 panels over

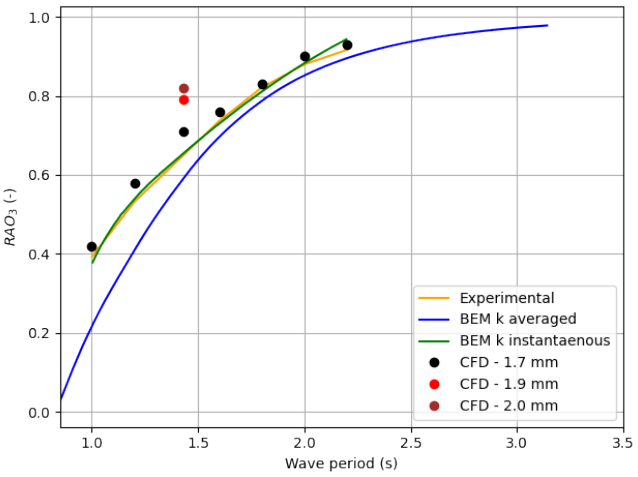

Fig. 17. Response amplitude operator (RAO) obtained with experiments, BEM and CFD modelling

the OWC hull and the imaginary piston together for 150 frequencies between 2 and 5 rad/s was close to 6 hours. These simulations were performed on a 8 core laptop with i7 processor with 16 GB of RAM. No parallelization was implemented. The simulations for 150 frequencies was performed particularly for the sensitivity analysis. If we were to consider just cases H01-H10 (7 different wave periods), then the simulation time was close to 20 minutes.

The computational time needed for the simulations in the CFD-NWT is around 48 h for a simulation time for the ten cases considered with a 16 cores MPI run on a i9 desktop PC with 64 GB of RAM. The high computational requirements of CFD simulations, also in this two-dimensional application, are mainly related to the need to discretize the very small slit on the OWC top cover (V=1.7 mm), i.e. reducing the size of the cells to tenths of mm in the zone characterized by the highest air velocities. The need to satisfy the aforementioned limitations on the Courant number Co, in turn, implies a drastic decrease of the computational time step when the velocity of the airflow in/out the OWC chamber peaks.

VII. Summary and Conclusions

Two numerical models are developed to model a box-type bottom-detached OWC - 1) A three-dimensional frequency domain model based on BEM using open-source solver Nemoh which uses an averaged linear damping coefficient relating the pressure and discharge, 2) A two-dimensional CFD-NWT allowing for wave generation and absorption implemented within the open-source package OpenFOAM. These two models are compared with the experimental results for ten test cases and the compared parameters include the displacement of the free surface within the OWC, the pressure above the free surface, the RAOs and the computational time.

Results for the displacement of the free surface show that for the BEM model, the relative error in the displacement of the free surface with respect to the experiments were as high as 16% while with the CFD-NWT, the highest relative error was close to 7% when comparing with the experiments. Similar trend is observed for the relative error in the pressure above the free surface wherein it is a peak of 20% for BEM while it is a peak of 14% for the CFD-NWT. This is further reflected in the RAO for the free surface, which shown the the results from the CFD-NWT are close to the experiments when considering a slit size of 1.7 mm while the BEM model with the average linear damping coefficient underestimates the response.

To further improve the results from the BEM model, an instantaneous frequency dependent damping coefficient based on the experimental results is derived. This is seen to provide results close to the experiments similar to the CFD-NWT. A comparison is also made between the computational resources utilized by the two numerical methods. While a exact direct comparison cannot be made since the calculations from the two methods were performed in two different computers, it is reasonable to say that the computations from the frequency domain BEM model based on the instantaneous damping coefficient will be much faster than the CFD-NWT computations for this application.

VIII. Acknowledgements

The work has received funding from EU-SCORES project under the European Union's Horizon 2020 research and innovation programme under grant agreement No 101036457. The research contract of I. S. is co-funded by the European Union - PON Research and Innovation 2014-2020 in accordance with Article 24, paragraph 3a), of Law No. 240 of December 30, 2010, as amended, and Ministerial Decree No. 1062 of August 10, 2021.

References

[1] A. F. Falcão and J. C. Henriques, "Oscillating-water-column wave energy converters and air turbines: A review," *Renewable Energy*, vol. 85, pp. 1391–1424, 2016. [Online]. Available: https://www.sciencedirect.com/science/article/pii/S0960148115301828

[2] Y. Delauré and A. Lewis, "3D hydrodynamic modelling of fixed oscillating water column wave power plant by a boundary element methods," *Ocean Engineering*, vol. 30, no. 3, pp. 309–330, 2003. [Online]. Available: https://www.sciencedirect.com/science/article/pii/S002980180200032X

[3] H. B. Bingham, D. Ducasse, K. Nielsen, and R. Read, "Hydrodynamic analysis of oscillating water column wave energy devices," *Ocean Engineering and Marine Energy*, vol. 1, p. 405–419, 2015. [Online]. Available: https://link.springer.com/article/10.1007/s40722-015-0032-4

[4] W. Sheng, R. Alcorn, and A. Lewis, "Assessment of primary energy conversions of oscillating water columns. i. hydrodynamic analysis," *Renewable and Sustainable Energy*, vol. 6, 2014. [Online]. Available: https://aip.scitation.org/doi/10.1063/1.4896850

[5] M. Penalba, T. Kelly, and J. Ringwood, "Using NEMOH for modelling wave energy converters: A comparative study with WAMIT," in *12th European Wave and Tidal Energy Conference (EWTEC)*, 2017.

[6] F. Opoku, M. Uddin, and M. Atkinson, "A review of computational methods for studying oscillating water columns – the navier-stokes based equation approach," *Renewable and Sustainable Energy Reviews*, vol. 174, p. 113124, 2023. [Online]. Available: https://www.sciencedirect.com/science/article/pii/S136403212201005X

[7] A. Elhanafi, G. Macfarlane, A. Fleming, and Z. Leong, "Experimental and numerical investigations on the hydrodynamic performance of a floating–moored oscillating water column wave energy converter," *Applied Energy*, vol. 205, pp. 369–390, 2017. [Online]. Available: https://www.sciencedirect.com/science/article/pii/S0306261917310127

[8] I. Simonetti, L. Cappietti, H. Elsafti, and H. Oumeraci, "Optimization of the geometry and the turbine induced damping for fixed detached and asymmetric OWC devices: A numerical study," *Energy*, vol. 139, pp. 1197–1209, 2017. [Online]. Available: https://www.sciencedirect.com/science/article/pii/S0360544217314111

[9] L. Carlo, C. Iuppa, and C. Faraci, "A numerical-experimental study on the hydrodynamic performance of a U-OWC wave energy converter," *Renewable Energy*, vol. 203, pp. 89–101, 2023. [Online]. Available: https://www.sciencedirect.com/science/article/pii/S0960148122018420

[10] Z. Deng, C. Wang, P. Wang, P. Higuera, and R. Wang, "Hydrodynamic performance of an offshore-stationary OWC device with a horizontal bottom plate: Experimental and numerical study," *Energy*, vol. 187, p. 115941, 2019. [Online]. Available: https://www.sciencedirect.com/science/article/pii/S0360544219316251

[11] L. A. Gaspar, P. R. Teixeira, and E. Didier, "Numerical analysis of the performance of two onshore oscillating water column wave energy converters at different chamber wall slopes," *Ocean Engineering*, vol. 201, p. 107119, 2020. [Online]. Available: https://www.sciencedirect.com/science/article/pii/S0029801820301840

[12] I. Simonetti and L. Cappietti, "Hydraulic performance of oscillating water column structures as anti-reflection devices to reduce harbour agitation," *Coastal Engineering*, vol. 165, p. 103837, 2021. [Online]. Available: https://www.sciencedirect.com/science/article/pii/S0378383920305238

[13] A. Iturrioz, R. Guanche, J. Lara, C. Vidal, and I. Losada, "Validation of OpenFOAM® for oscillating water column three-dimensional modeling," *Ocean Engineering*, vol. 107, pp. 222–236, 2015. [Online]. Available: https://www.sciencedirect.com/science/article/pii/S0029801815003649

[14] I. Simonetti, L. Cappietti, H. Elsafti, and H. Oumeraci, "Evaluation of air compressibility effects on the performance of fixed owc wave energy converters using cfd modelling," *Renewable Energy*, vol. 119, pp. 741–753, 2018. [Online]. Available: https://www.sciencedirect.com/science/article/pii/S0960148117312235

[15] M. Shalby, A. Elhanafi, P. Walker, and D. G. Dorrell, "CFDmodelling of a small–scale fixed multi–chamber OWC device," *Applied Ocean Research*, vol. 88, pp. 37–47, 2019. [Online]. Available: https://www.sciencedirect.com/science/article/pii/S0141118718307855

[16] A. Babarit and G. Dolhommeau, "Theoretical and numerical aspects of the open source BEM solver NEMOH," in *11th European Wave and Tidal Energy Conference (EWTEC2015)*, 2015.

[17] W. Sheng, E. Tapoglou, X. Ma, C. Taylor, R. Dorrell, D. Parsons, and G. Aggidis, "Hydrodynamic studies of floating structures: Comparison of wave-structure interaction modelling," *Ocean Engineering*, vol. 249, p. 110878, 2022. [Online]. Available: https://www.sciencedirect.com/science/article/pii/S0029801822003183

[18] D. Kisacik *et al.*, "Efficiency and survivability of a floating oscillating water column wave energy converter moored to the seabed: An overview of the EsflOWC MaRINET2 database," *Water*, vol. 12, no. 4, 2020. [Online]. Available: https://www.mdpi.com/2073-4441/12/4/992

[19] T. L. W. Sheng and R. Alcorn, "On wave energy extraction of oscillating water column device," in *4th International Conference on Ocean Energy*, 2012.

[20] B. Le Méhauté, "An introduction to hydrodynamics and water waves," *Springer*, 1976.

[21] C. Hirt and B. Nichols, "Volume of fluid (vof) method for the dynamics of free boundaries," *Journal of Computational Physics*, vol. 39, no. 1, pp. 201–225, 1981. [Online]. Available: https://www.sciencedirect.com/science/article/pii/0021999181901455

[22] P. Higuera, J. L. Lara, and I. J. Losada, "Realistic wave generation and active wave absorption for navier–stokes models: Application to openfoam®," *Coastal Engineering*, vol. 71, pp. 102–118, 2013. [Online]. Available: https://www.sciencedirect.com/science/article/pii/S0378383912001354

[23] B. E. Larsen and D. R. Fuhrman, "On the over-production of turbulence beneath surface waves in reynolds-averaged navier–stokes models," *Journal of Fluid Mechanics*, vol. 853, p. 419–460, 2018.

[24] L. Cappietti and I. Simonetti, "On the effectiveness of oscillating water column devices in reducing the agitation in front of vertical walls harbor structures," in *Coastal Engineering Proceedings*, 2018.

[25] A. Sarmento, L. Gato, and A. de O. Falcão, "Turbine-controlled wave energy absorption by oscillating water column devices," *Ocean Engineering*, vol. 17, no. 5, pp. 481–497, 1990. [Online]. Available: https://www.sciencedirect.com/science/article/pii/002980189090040D

[26] B. N. Fox, R. P. Gomes, and L. M. Gato, "Analysis of oscillating-water-column wave energy converter configurations for integration into caisson breakwaters," *Applied Energy*, vol. 295, p. 117023, 2021. [Online]. Available: https://www.sciencedirect.com/science/article/pii/S0306261921004876

[27] J. Henriques, J. Portillo, L. Gato, R. Gomes, D. Ferreira, and A. Falcão, "Design of oscillating-water-column wave energy converters with an application to self-powered sensor buoys," *Energy*, vol. 112, pp. 852–867, 2016. [Online]. Available: https://www.sciencedirect.com/science/article/pii/S0360544216308283

[28] W. Sheng and G. Aggidis, *Fundamentals of Wave Energy Conversions: The Dynamics of the Wave-Structure Interactions and Wave Energy Optimisation*. Eliva press, 2022. [Online]. Available: https://www.elivapress.com/en/book/book-3680559883/